Received: 24 July 2024 | Revised: 16 September 2024 | Accepted: 20 September 2024

https://doi.org/10.1016/j.jtha.2024.09.026

ISTH SSC COMMUNICATIONS

Recommendations for defining disturbed flow as laminar, transitional, or turbulent in assays of hemostasis and thrombosis: communication from the ISTH SSC Subcommittee on Biorheology

David L. Bark[1] | Eudorah F. Vital[2] | Cécile Oury[3] | Wilbur A. Lam[2,4] | Elizabeth E. Gardiner[5]

[1]Department of Pediatrics, Division of Hematology and Oncology, Washington University in St. Louis, St. Louis, Missouri, USA

[2]Wallace H. Coulter Department of Biomedical Engineering, Georgia Institute of Technology and Emory University School of Medicine, Atlanta, Georgia, USA

[3]GIGA Metabolism and Cardiovascular Biology – Laboratory of Cardiology, University of Liège, Liège, Belgium

[4]Aflac Cancer and Blood Disorders Center of Children's Healthcare of Atlanta, Department of Pediatrics, Emory University School of Medicine, Atlanta, GA, USA

[5]Division of Genome Science and Cancer, The John Curtin School of Medical Research, The Australian National University, Canberra, ACT, Australia

Correspondence
David L. Bark, Division of Hematology & Oncology, Department of Pediatrics, Campus Box 8116, 660 South Euclid Ave, Saint Louis, Missouri 63110, USA.
Email: bark@wustl.edu

Funding information
D.L.B. acknowledges funding support from the National Heart, Lung, and Blood Institute (R01HL164424); and National Institute of Biomedical Imaging and Bioengineering (R21EB034579). E.E.G. receives funding from the National Health and Medical Research Council of Australia.

Abstract

Blood flow is vital to life, yet disturbed flow has been linked to atherosclerosis, thrombosis, and endothelial dysfunction. The commonly used hemodynamic descriptor "disturbed flow" found in disease and medical devices is not clearly defined in many studies. However, the specific flow regime—laminar, transitional, or turbulent—can have very different effects on hemostasis, thrombosis, and vascular health. Therefore, it remains important to clinically identify turbulence in cardiovascular flow and to have available assays that can be used to study effects of turbulence. The objective of the current communication was to 1) provide clarity and guidance for how to clinically identify turbulence, 2) define standard measures of turbulence that can allow the recreation of flow conditions in a benchtop assay, and 3) review how cells and proteins in the blood can be impacted by turbulence based on current literature.

KEYWORDS
arteries, blood flow velocities, hemodynamics, rheology, turbulence

Manuscript handled by: Kathleen Freson

Final decision: Kathleen Freson, 20 September 2024

1 | INTRODUCTION

Pathophysiological blood flow is known to affect hemostasis and thrombosis [1–4]. Although most, if not all, physiological flow is laminar, pathophysiological disturbed flow can be stable laminar, unstable laminar, transitional, or even turbulent, with the latter characterized by high-frequency fluctuations in fluid velocity and pressure leading to chaotic flow patterns. Despite its reported effects on hemostasis and thrombosis, unstable laminar (disturbed) flow is commonly mischaracterized as turbulent in the blood literature. The following sections provide an overview of the fundamental fluid dynamics that underpin turbulent blood flow compared with unstable laminar flow, metrics of turbulence, and techniques used to quantify blood flow instability. Lastly, we outline assays that have been developed to generate highly unstable flow and how these have been used to show the impact on proteins and cells. Overall, this communication provides guidance for the topic of turbulence in the context of hemostasis and thrombosis.

2 | TURBULENCE IN A STRAIGHT, SMOOTH VESSEL

Stable laminar flow through an idealized blood vessel, depicted as a straight, smooth cylinder, results in fluid particles or blood cells that follow a straight path parallel to the walls without mixing into surrounding layers, as can be demonstrated by injecting a dye into the flow (Figure 1A). With increased velocity, fluid inertia becomes larger, making it more difficult for fluid viscosity to dampen out fluctuations within the flow, leading to transitional flow. For transitional flow, injected dye begins to deviate from a straight line (Figure 1B) with intermittent regions of velocity and pressure fluctuations but little to no mixing of the dye with the surrounding fluid. Further increases in fluid speed can lead to turbulence, where the dye rapidly mixes with surroundings due to multiscale velocity and pressure fluctuations (Figure 1C). There is a nondimensional (unitless) number that quantifies the fluid inertia (numerator) relative to viscous dissipation (denominator) to help identify these 3 flow regimes, known as the Reynolds number (*Re*):

$$Re = \frac{\rho U D}{\mu}, \qquad \text{Equation 1}$$

where ρ is the fluid density, U is the fluid velocity, D is the diameter of the vessel or length scale of the flow, and μ is the viscosity. Generally, in a smooth pipe, flow is laminar for $Re \leq 2000$, transitional for $2000 < Re \leq 4000$, while $Re > 4000$ leads to turbulence. The *Re* leading to turbulence is commonly termed the critical *Re*. However, *Re* values defining these 3 regimes are not universal but instead provide guidance. Critical *Re* decreases with surface roughness or if flow decelerates through pulsatility or a disturbance [5].

The velocity profile and wall shear stress depend on whether flow is laminar or turbulent. Far from flow disturbances, blood velocity nearly follows a parabolic distribution but is slightly blunted due to rheological behavior of whole blood, with zero velocity at the vessel wall and a maximum velocity at the center of the vessel (Figure 2A). Simplified to a parabolic profile, this leads to an estimated wall shear stress of $\tau = 4\mu Q/\pi R^3$, where Q is the flow rate. Resultingly, the pressure drop across the length of the vessel is proportional to the flow rate. In turbulence, fluid particles (or blood cells) move from low- to high-velocity layers of fluid, and vice versa, while carrying fluid

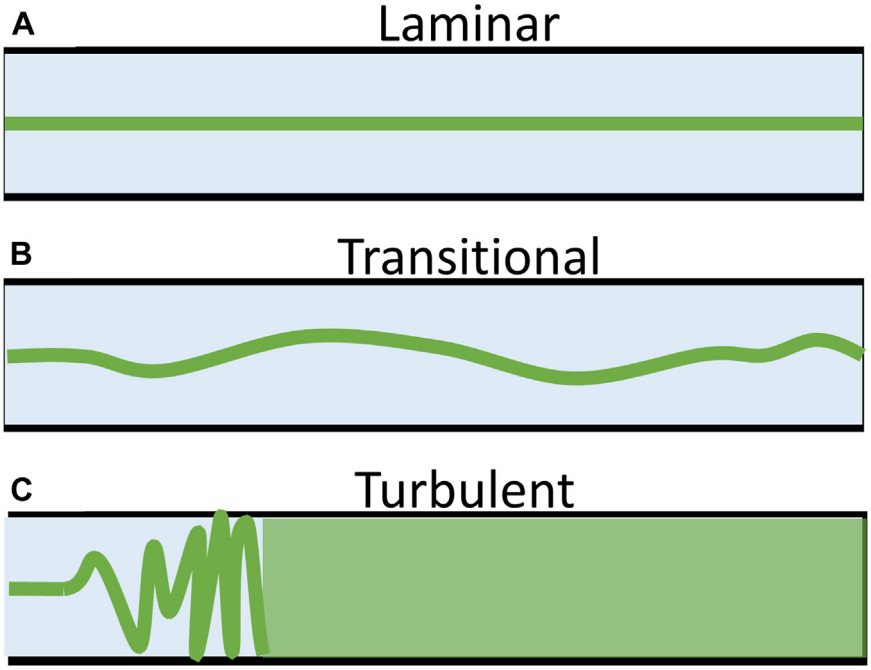

FIGURE 1 Representation of flow regimes with an illustration of how dye injected at the center of a straight tube may vary through the tube. In (A) laminar flow, the dye follows a straight path down the center of the vessel. For (B) transitional flow, intermittent fluctuations in velocity cause the dye to deviate from the straight path without mixing with surrounding fluid layers. For (C) turbulent flow, the dye quickly mixes and disperses with surrounding fluid due to sustained velocity fluctuations.

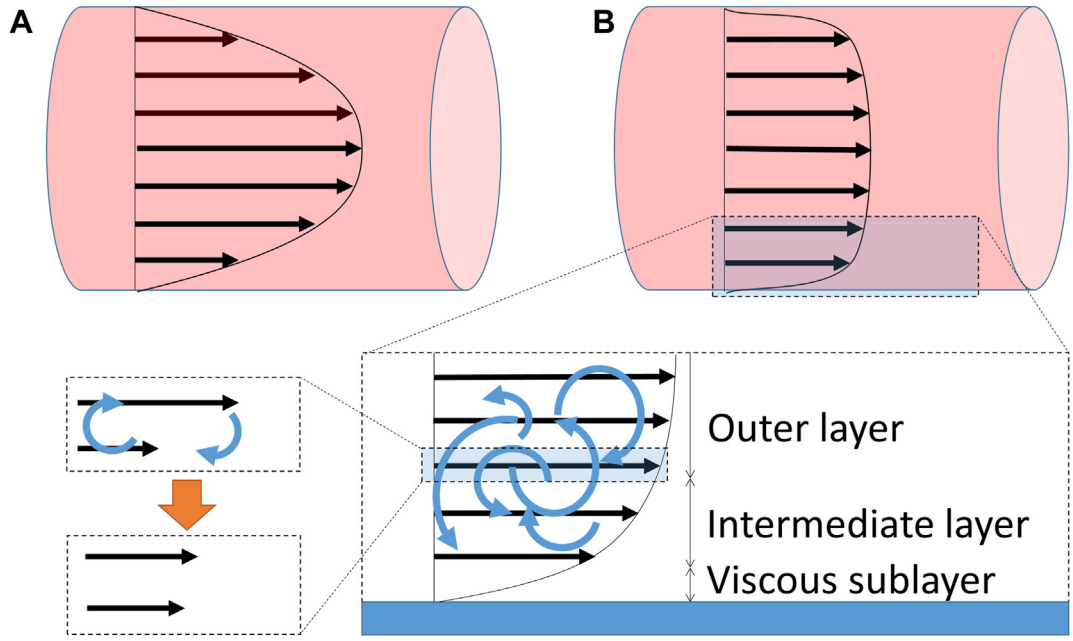

FIGURE 2 Illustration of the velocity profile for (A) laminar flow and (B) turbulent flow. Within turbulent flow, momentum is exchanged across fluid layers as particles carrying momentum move across the layers. The blue arrows illustrate the exchange of fluid momentum that causes higher velocity layers to decrease in speed with lower velocity layers increasing in speed, thereby normalizing the velocity in the outer layer of fluctuating velocity and pressure. The velocity gradient becomes very sharp in the intermediate region that transitions flow to the laminar viscous sublayer as velocity slows to 0 at the wall.

momentum to neighboring fluid layers, ultimately making the profile more blunted. The profile change causes a very sharp velocity gradient at the vessel wall (Figure 2B) and an increased wall shear stress that increases nonlinearly with *Q*, thereby requiring a greater pressure drop to drive flow across the length of the vessel. The very thin layer closest to the wall, with the sharp velocity gradient, is known as the viscous sublayer, where flow behavior is dominated by viscosity. Away from the wall is the outer layer, where turbulence and mixing are prevalent, with an intermediate layer transitioning between the other 2.

3 | DEFINING FLOW REGIMES

Stable laminar, transitional, and turbulent flows are described above. Unstable laminar flow or disturbed flow is often misunderstood or misdefined as turbulent in blood literature. Unstable laminar flow occurs when disturbances to blood flow, eg, bifurcations, aneurysms, large vessel curvature, or stenosis, are amplified, yet flow maintains regularity without irregular fluctuations. Regularity means that fluid repeatably follows the same paths that are not necessarily parallel to the vessel wall with each cardiac cycle. Any sudden change in geometry can cause unstable laminar flow if the *Re* is sufficiently high. Despite the elevated *Re*, unstable laminar flow is not turbulent.

Multiple types of rotational flow features can form for unstable laminar flow. In geometrical expansions, eg, aneurysms, stenotic geometry, or sinuses (Figure 3A), inertial forces carry fluid forward, meaning that fluid particles can locally travel away from the wall of the expansion, known as flow separation, which leads to recirculation (flow reversal at the wall). Another feature forms at the aortic arch (Figure 3B) due to extreme vessel curvature at a large *Re*. Centrifugal forces cause "secondary flow" perpendicular to the primary flow with counterrotating vortices known as Dean vortices. This weaker secondary flow leads to a helical flow path for blood since the primary flow simultaneously carries fluid forward. Flow can even separate near the inner bend of the aorta as the velocity profile becomes skewed toward the outer curvature. Another nondimensional number, the Dean number (*De*), can be used to predict the amount of secondary flow, defined as:

$$De = Re\sqrt{\frac{D}{2R_c}}, \qquad \text{Equation 2}$$

where *D* is the diameter of the vessel, and R_c is the radius of curvature, depicted in Figure 3B. $De<\sim40$ is unidirectional. Above this, Dean vortices can begin to form. If *De* becomes sufficiently high ($De>\sim650$), velocity fluctuations can occur with evidence of weak turbulence [6]. To further demonstrate unstable laminar flow, Figure 4A (6–8) shows flow with dye through a glass model of the carotid sinus. This flow is not turbulent since these parallel helical flow paths are smoothly varying and repeatable. Furthermore, the tracer dye does not rapidly mix into surrounding fluid, which would otherwise occur in turbulent flow. Vortices in unstable laminar flow are shown in Figure 4B. These become irregular and wavy if the *Re* continues to increase (Figure 4C) until transitioning into turbulence (Figure 4D) [6].

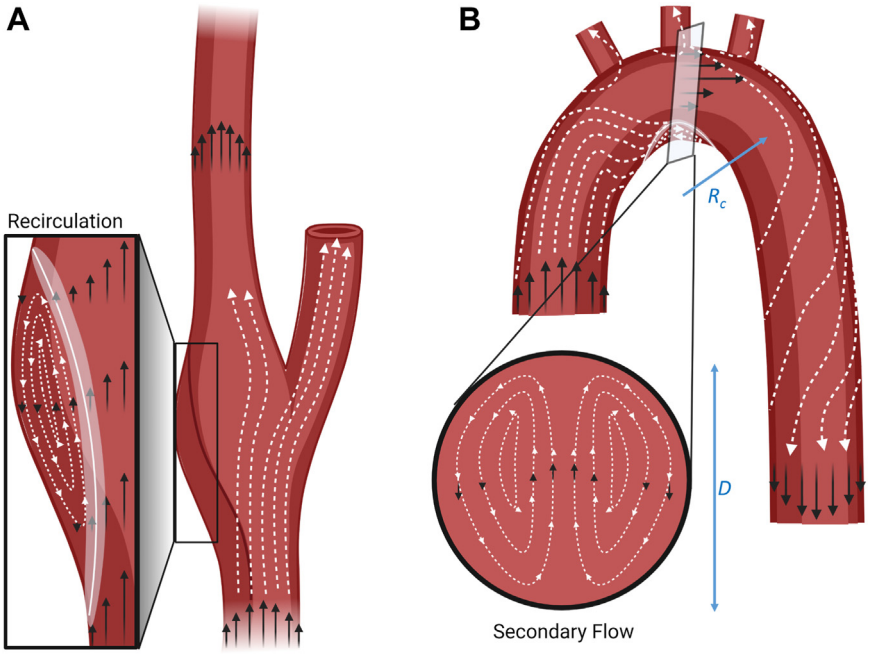

FIGURE 3 (A) An illustration of flow separation at the carotid sinus. In flow separation, flow reverse direction at the vessel wall creating a region of flow recirculation. A dividing streamline forms away from the wall, separating the recirculation region from the rest of the flow. The highest shear in the flow is free from the bounds of the vessel wall, which can lead to 3-dimensional vorticity and flow instability that triggers turbulence. (B) An illustration of flow separation and secondary flow in the aortic arch. Secondary flow is a weaker flow compared with the primary axial flow but can cause meandering fluid particle pathlines. In this example, D is the diameter of the vessel, and R_c is the radius of curvature, which can be combined with the Reynolds number to characterize the amount of secondary flow.

4 | PARAMETERS FOR DEFINING TURBULENCE

In turbulent flow, the velocity (and pressure) fields experience random fluctuations, which can be quantified through statistics. A mathematical technique known as Reynolds decomposition separates the fluid velocity into mean behavior and fluctuations around the mean, as described by the following equation:

$$U(t) = \overline{U}(t) + u(t), \qquad \text{Equation 3}$$

where $\overline{U}(t)$ is the mean velocity at a point in the cardiac cycle where the overbar denotes that the variable is averaged, and $u(t)$ is the turbulent velocity fluctuation about the mean. Parameter t represents time, and both the velocity mean and fluctuations can be a function of time for pulsatile flow, as demonstrated by the parentheses. In the current explanation, we consider velocity only in 1 spatial dimension at a single point in space for simplicity, although it is actually 3-dimensional (3D) and can vary in space. For steady flow, $\overline{U}$ is constant, without variations in time (Figure 5A). However, $u(t)$ is random, thereby fluctuating in time. Fluctuations can be characterized by a probability density function. For pulsatile, periodic cardiovascular flow, the flow repeats each cardiac cycle, and therefore, an "ensemble averaged" $\overline{U}(t)$ can be calculated, meaning the average is taken at multiple time points within a cardiac cycle over many cycles (Figure 5B; black curve). To ensure accuracy, the number of cycles should be increased until $\overline{U}(t)$ no longer changes with additional cycles, typically requiring hundreds of cycles. A separate probability density function of $u(t)$ will exist at each time point throughout the cycle period.

4.1 | Parameters for quantification of turbulence

Turbulent kinetic energy (TKE) provides the mean energy per unit mass generated by turbulent flow, ie, the kinetic energy per unit mass from velocity fluctuations. It is calculated from the mean of the squares of the fluctuating velocity component in all directions:

$$TKE = \frac{1}{2}\left(\overline{u(t)^2} + \overline{v(t)^2} + \overline{w(t)^2}\right), \qquad \text{Equation 4}$$

where v and w are velocity fluctuations in the 2 directions perpendicular to u. Typical values are described below. Again, note that the overbar indicates that averages are taken of terms below it. TKE is a scalar that varies in space, and for pulsatile flow, it can vary in time. Depending on the study, TKE is also sometimes reported as the kinetic energy per unit volume, $\rho\overline{u(t)^2}$, or the square root of the energy per unit mass, $\sqrt{\overline{u(t)^2}}$, represented in 1 dimension here. It is also salient to consider the spatially varying and time-varying Reynolds shear stress (RSS) with units of stress, eg, dynes/cm^2 or Pa:

$$RSS = \rho\overline{u(t)v(t)}, \qquad \text{Equation 5}$$

where $v(t)$ is the root mean square of the turbulent velocity fluctuations perpendicular to $u(t)$. RSS may be misleading because it is not a real stress. Instead, it is a consequence of inserting Equation 2 into the governing equations for fluid mechanics, ie, the Navier–Stokes equations, and is the only remaining term that accounts for velocity fluctuations. Despite it being only a mathematical outcome, as opposed to real stress, theoretical arguments based on scaling relate the RSS to the instantaneous shear stress in blood [9,10], providing possible explanations for how RSS is related to hemolysis. Lastly,

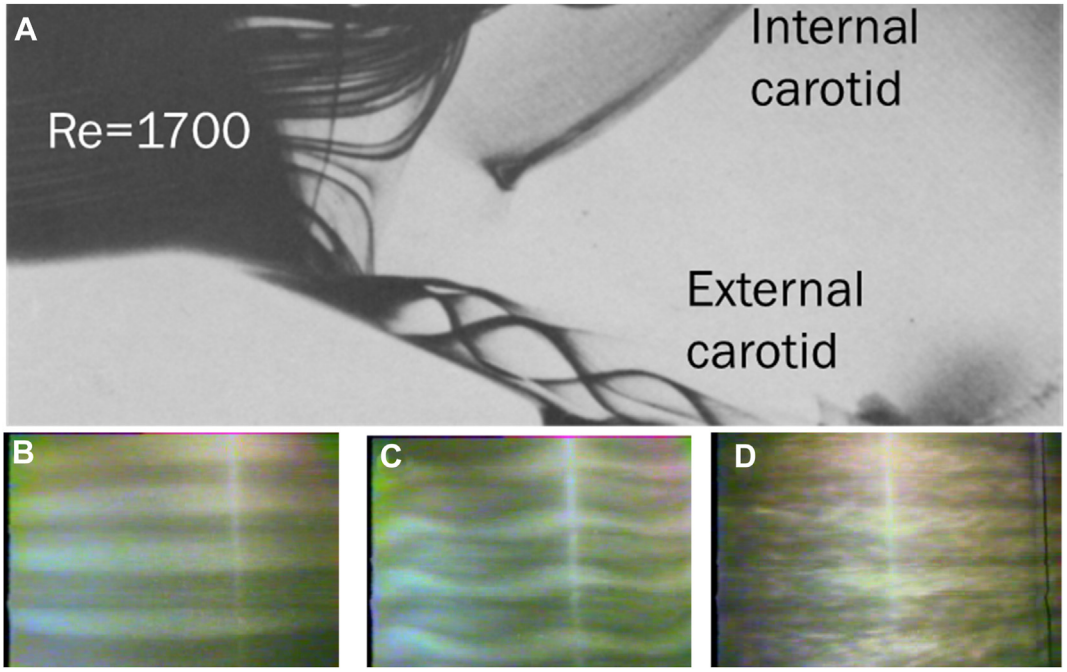

FIGURE 4 (A) Flow visualization using a glass model of the carotid sinus showing flow separation and helical flow patterns, reprinted from Bharadvaj et al. [7] with permission. This is not turbulent flow. The bottom panels are reprinted from Aider et al. [6] with permission and demonstrate vortex progression from unstable laminar flow into turbulent flow using a cylinder rotating inside another transparent cylinder, an observation first made in the early 1900s [6,8]. The view is from the side of the outer cylinder with different shades pertaining to vortices rotating in opposing directions. The images represent (B) Taylor vortices, (C) wavy vortex flow, and (D) weak turbulence. Note that the turbulent flow consists of multiple spatial scales that will be discussed in 4.2 scales in turbulence. *Re*, Reynolds number.

turbulence intensity (*TI*) is sometimes used to quantify the amount of turbulence:

$$TI = \frac{\sqrt{\frac{1}{3}\left(\overline{u(t)^2} + \overline{v(t)^2} + \overline{w(t)^2}\right)}}{\sqrt{\overline{U}(t)^2 + \overline{V}(t)^2 + \overline{W}(t)^2}}. \qquad \text{Equation 6}$$

As a general estimation, values less than 1% are considered low, 1% to 5% medium, and greater than 5% is considered a high amount of turbulence. For Equations 4 to 6, maximum or averaged (in time and/or space) values may be reported in the literature. It should be noted that data may be taken over 1 or 2 dimensions, as opposed to 3, due to inherent limitations of measurement techniques. This can lead to an

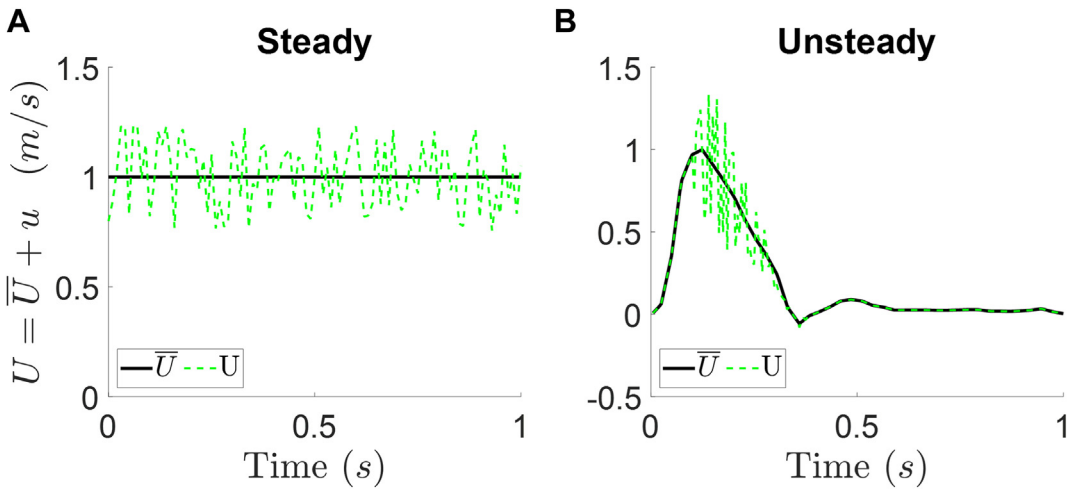

FIGURE 5 Depiction of the Reynolds decomposition that splits the instantaneous velocity (green dashed line) into an average (black solid line) and fluctuating value, noting that the fluctuating value is the difference between the green and black lines. This can be done for (A) steady flow that does not change in time where the average velocity is a constant and (B) unsteady (pulsatile) flow that does change in time where the average velocity curve also changes in time for a single cardiac cycle. *U* is the instantaneous velocity; $\overline{U}$, is the time-averaged velocity, which involves an ensemble average for unsteady flow, and *u* is the turbulent velocity fluctuation about the mean.

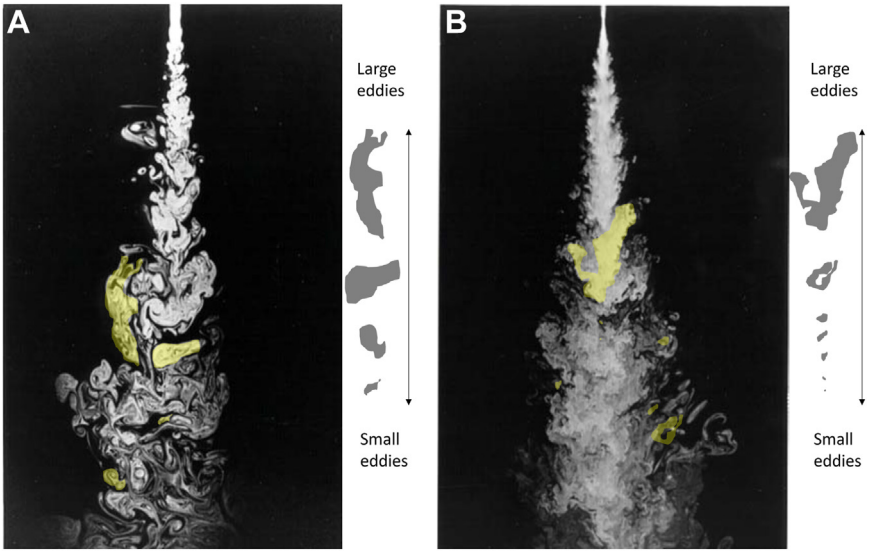

FIGURE 6 Turbulent jets at (A) Reynolds number (*Re*) ≅ 2.5×10^3 and (B) *Re* ≅ 1.0×10^4 visually depicting eddies and demonstrating that the range of eddy length scales increases for increasing *Re*, reprinted and modified from Dimotakis [12] with permission. At the lower *Re*, medium to large eddies are seen, as represented by the large, clearly visible white structures. At the higher *Re*, these same structures exist, but with smaller structures within these larger structures. Due to the presence of the smaller eddies, it makes the larger eddy boundaries less discernable. In addition, the smallest eddies are below the image resolution for the high *Re* condition.

underestimation of values, and therefore, care must be taken when interpreting and comparing among multiple studies.

4.2 | Scales in turbulence

Length and time scales found in turbulence are important in hemostasis and thrombosis and are fundamental to identifying turbulence [11]. These scales can be conceptualized through Kolmogorov's theory of turbulence, which proposes an "energy cascade," where mixing fluid sections, termed "eddies," transfer energy from flow at the vessel scale to smaller eddies until a minimal scale where viscosity dissipates energy into heat or potentially cellular and protein deformation in the case of blood. The smallest eddies predicted from a Kolmogorov length scale can approach the size of a cell in turbulent cardiovascular flows [1,10]. It is unlikely that eddies could occur at smaller scale than a red blood cell (RBC) since plasma must squeeze through rotating RBCs, and for this scale, the *Re* becomes very small [9]. To help the reader visualize the length scales associated with Kolmogorov's theory of turbulence, a broad spectrum of turbulent spatial scales can be seen in the fluid extending from a jet in Figure 6 (12), where the range of spatial scales increases with increasing *Re* (Figure 6A vs B). These scales can also be seen in Figure 4D.

Temporal scales are also found with turbulent flow. Kolmogorov's theory suggests that small energy-dissipating eddies have a shorter time scale compared with large eddies. Time scales can be seen with high-frequency velocity and pressure fluctuations (>100 Hz) in flow, eg, frequencies much greater than the ~1 Hz cardiac cycle. These time scales could influence time-dependent cell and protein deformation in response to stresses. If fluctuations are faster than the deformation, behavior may differ compared with fluctuations that are slower than the deformation. As a hypothetical example, von Willebrand factor (VWF) is understood to stretch and recoil to a globular confirmation in certain flows. If fluctuations are too fast, VWF may not have time to fully stretch or fully recoil, compared with flow that changes speed slowly. This behavior has been demonstrated with DNA and polymers by imaging single strands and comparing extension at low- and high-frequency oscillations [13,14]. When using temporal fluctuations to identify turbulence, it is critical to distinguish the fluctuations from noise in the measurement technique.

5 | TOOLS TO IDENTIFY AND QUANTIFY TURBULENCE

Quantifying turbulence in circulation is fraught with challenges, primarily because high temporal and spatial resolution techniques are needed and must be distinguished from measurement noise.

5.1 | *In silico*

Computational fluid dynamics (CFD) is commonly performed to characterize patient-specific cardiovascular flow. Although CFD is robust for quantifying fluid velocity distributions and shear stress in laminar flow, it requires significantly more care when modeling turbulence. Most turbulence models require *a priori* knowledge of whether a flow is turbulent. These methods can be useful for matching parameters like TKE to a patient population and for quantifying average flow behavior. The only accepted computational way to detect the potential presence of turbulence at all scales is through direct numerical simulation, requiring very fast computers and months to years to process a single simulation and is therefore impractical for most studies in hemostasis and thrombosis, especially considering the complex rheology of blood.

5.2 | *In vivo*

Several noninvasive and minimally invasive methods have been developed to identify turbulence in the cardiovascular system.

Magnetic resonance imaging (MRI) is commonly used for this purpose [15–18]. Magnetic resonance velocimetry provides a way to obtain a detailed flow field that has been experimentally validated [19]. However, it is important to note that MRI is limited in resolution to roughly 1 mm^3 voxels. Comparatively, the aortic diameter is roughly 1 inch or 24 mm. In addition to limited resolution, sources of error for MRI generally stem from noise, where turbulence may be poorly estimated for a low signal-to-noise ratio [20]. Doppler ultrasound provides another technique for quantifying turbulence [21,22]. This approach is limited to quantification in the direction of the ultrasound beam. Although useful for identifying high-frequency fluctuations, it is challenging, if even possible, to extract quantitative parameters like TKE since motion from the probe or tissue, eg, breathing, could lead to measurement variations between cardiac cycles. Minimally invasive single-point measurements through hot film anemometry can be used by placing the probe into circulation via a catheter [2]. This technique provides local accurate blood velocity measurements if care is taken to avoid contamination of the probe by fibrin or adherent platelets. Although *in vivo* methods can most directly identify and quantify turbulence, each technique comes with drawbacks. Also, as noted earlier, accurate quantification of turbulence requires repeated measurements over many cardiac cycles, yet *in vivo* methods are typically constrained to a small number to remain practical.

5.3 | *In vitro*

In vitro systems can vary, depending on the goal of the system, but typically involve patient-specific or idealized vascular anatomy where the flow field (spatial and temporal velocity detail) can be thoroughly quantified (Figure 4A). Patient anatomy can be recreated with an optically transparent material, eg, silicone, glass, or polycarbonate, to enable light-dependent measurement methods, while fluid is pumped through the anatomy to replicate patient flow. Laser Doppler anemometry or velocimetry is a very accurate method for making point measurements of velocity and/or turbulence in these systems [23]. It leverages the Doppler shift in a laser beam that depends on the velocity of a fluid but requires optical access to the fluid to make measurements. Two additional techniques include particle imaging velocimetry (PIV) and particle tracking velocimetry (PTV). In both, particles are seeded into a flow and are observed with a high-speed camera (from thousands to tens of thousands of frames per second) while particles are illuminated. PIV correlates fragments of an image between frames to quantify local regions of particle displacement, while PTV tracks individual particles based on features of the particles. Both methods quantify the spatial and temporal distribution of fluid velocity with very high resolution. Furthermore, flow in these systems can be identically repeated hundreds of times, supporting statistical methods for quantifying turbulence. *In vitro* experiments also lend themselves to qualitative flow visualization.

6 | WHERE CAN TURBULENCE EXIST IN THE CIRCULATION?

Re must be high for turbulence to occur in circulation and therefore should only be found in the great vessels of arterial flow, if anywhere. Although disturbed blood flow is not typically turbulent, flow separation and secondary flow can aid the development of turbulence due to 3D vorticity that is otherwise dampened out by the vessel wall. Flow deceleration due to pulsatility is also more likely to cause instability compared with acceleration, meaning turbulence is most likely at peak systole or early diastole. The following sections describe reported locations of turbulence.

6.1 | Healthy circulation

The left ventricle generates flow with a large *Re*, with signs of turbulence [24–26]. In the early filling phase of diastole (the E-wave), a jet is formed at the mitral valve that then breaks down in the diastasis phase (midportion of diastole), after which a second jet is formed in the atrial contraction phase (the A-wave). The 2 successive jets create shear layers that lead to vortex rings, which break down into coherent structures, ie, organized patterns of fluid motion that represent regions of concentrated energy or vorticity (fluid rotation). The vortex is a characteristic of unstable flow. *TKE* can reach 0.15 m^2/s^2 (Table 1) [2,22,27–32], corresponding to a large *TI*, with characteristic frequencies up to 200 Hz [27].

Due to the high *Re* (*Re*>4000), extreme curvature (*De* of ~600, leading to secondary flow), and the flow out of the left ventricle, there is unstable secondary flow and the potential for turbulence in a healthy aorta. MRI and PIV lead to *TKE* values up to 0.3 m^2/s^2, whereas hot film anemometry and Doppler ultrasound lead to a *TKE* that is an order of magnitude lower (Table 1) [2,22,30–32]. *TI* is found to reach up to 20%, depending on the measurement approach. Inconsistencies across studies can be a limitation of the measurement quality, the location of the measurement, the number of cardiac cycles used for a measurement, and the number of dimensions used to calculate *TKE*. MRI and PIV studies can spatially capture a whole flow field, making it straightforward to find maximum and spatially averaged *TKE* values compared with single-point measurement techniques. Furthermore, dominant frequencies of 100 to 300 Hz occur in the aorta, further supporting the presence of turbulence [2,32]. Although there are conflicting data, most studies show highly unstable, potentially turbulent flow in the aorta.

The carotid arteries have a *Re* that reaches above 1200 to 1700 at peak systole. Studies show unstable laminar flow separation and secondary flow (Figure 4) [7]. The carotid siphon, a tortuous vessel segment that is part of the internal carotid artery, with blood flows of *Re* 300 to 400, in some cases, can exhibit mild flow instabilities with dominant frequencies of 100 to 500 Hz [33]. Studies demonstrate very low *TKE* values (0.0002 m^2/s^2) based on 3D PIV measurements

TABLE 1 Turbulent kinetic energy measured or simulated under healthy physiological conditions.

Location	TKE (m^2/s^2)	Method	Ref
Left ventricle	0.15	MRI	[27]
Right ventricle	0.05-0.35	MRI	[28,29]
Aorta	0.12-0.3	PIV	[30]
	0.0009-0.01	Doppler ultrasound	[22]
	0.006-0.22	MRI	[31]
	0.0004-0.03	Hot film anemometry (canine and human)	[2,32]

MRI, magnetic resonance imaging; PIV, particle imaging velocimetry; Ref, reference; TKE, turbulent kinetic energy.

[34]. These and other distal vessels to the aorta are generally considered to have laminar or unstable flow but not turbulent flow.

6.2 | Pathologic circulation

Disease can increase the propensity for flow instability (Table 2) [22,35–46]. Cardiomyopathy (enlargement of cardiac muscle) can increase *TKE* [47]. Within the heart, mitral valve regurgitation (reverse flow) can lead to an elevated *TKE* in the ventricle [35]. This occurs when the mitral valve between the left atrium and ventricle fails to fully close during systole. When treated with a clip that holds leaflets together, CFD studies demonstrate coherent structures and a large degree of vorticity associated with these clips, suggesting an increased flow instability due to a restricted orifice area [48]. Poor performance of the aortic valve, located between the left ventricle and the aorta, can enhance turbulence in disease states. In aortic stenosis, the aortic valve does not fully open, thereby leading to a jet of fluid during systole with a large pressure gradient across a small orifice, ultimately causing >3× *TKE* values compared with a healthy aorta [36–38]. In aortic valve insufficiency, the aortic valve does not fully close, leading to regurgitant (reverse) flow through a small orifice during diastole, also resulting in elevated *TKE* [39]. The aorta can also narrow in the case of aortic coarctation, increasing the propensity for turbulent flow, with *TKE* values similar to those recorded in an aortic stenosis. Since the entire stroke volume flows through these regions, the potential of turbulence is relatively high compared with other vascular regions.

TABLE 2 Turbulent kinetic energy measured or simulated for pathologic circulation.

Condition	TKE (m^2/s^2)	Method	Ref
Mitral valve regurgitation	0.3	MRI	[35]
Aortic stenosis	0.3-1.0	MRI, CFD	[36–38]
Aortic valve insufficiency	0.3	MRI	[39]
Aortic coarctation	0.18-1.0	MRI, CFD	[39–42]
	<0.03	Doppler ultrasound	[22]
Carotid atherosclerosis	0.005-.05	CFD	[43,44]
Coronary atherosclerosis	<0.2	CFD	[45,46]

CFD, computational fluid dynamics; MRI, magnetic resonance imaging; Ref, reference; TKE, turbulent kinetic energy.

As noted, the carotid artery has disturbed flow. It can become more unstable in the presence of atherosclerotic plaque. A stenosis in the carotid artery can increase the instability of flow (Table 2) with an *RSS* of 6.15 Pa [43,44]. Coherent structures are also observed, along with frequency peaks reaching up to 300 Hz. Atherosclerosis is also found in coronary arteries. Although $Re<300$ in these vessels, plaque can cause flow to become unstable if the stenosis is severe enough [45,46,49–52]. However, these studies do not account for the reduction in flow associated with increased hydraulic resistance due to severe stenosis; therefore, findings should be interpreted cautiously [53]. Through models of atherosclerosis and MRI measurements, it is suggested that flow instabilities are possible, but turbulence might only exist in some extreme cases, if at all.

6.3 | Therapeutics

Various treatments for disease can also lead to turbulence (Table 3) [21,54–59]. Ventricular assist devices are used in patients with heart failure by supporting the ventricles to pump blood while reducing the load on the heart. However, high-speed rotors found in modern rotary ventricular assist devices can cause turbulence, with *TKE* levels that are similar to those observed in cardiac valve disease [54–56]. Valve disease itself is commonly treated with replacement or repair. Mechanical valves used for replacement, in some cases, are prone to low levels of turbulence or at least highly disturbed flow [60]. $TKE<0.15 m^2/s^2$ in bileaflet and trileaflet mechanical valves, with Kolmogorov length scales becoming as low as 25 μm, with a reported *RSS* of 35 Pa [61]. Studies specifically performed in the hinge region of a CarboMedics valve exhibit a turbulent shear stress of 564 Pa based on laser Doppler velocimetry [57]. Turbulence associated with bileaflet mechanical valves is qualitatively shown as coherent structures (Figure 7) [62]. More recently, transcatheter valves are gaining favor, but due to the nature of the surrounding stent, these exhibit high $TKE>0.3 m^2/s^2$ [59]. Therefore, many treatments for disease can lead to turbulent flow.

TABLE 3 Turbulent kinetic energy measured or simulated in medical devices.

Device	TKE (m^2/s^2)	Method	Ref
VADs			
HeartMate 3 (Abbott Cardiovascular)	0.30	CFD and PTV	[54,55]
HeartMate II (Abbott Cardiovascular)	>0.50o	CFD	[56]
HeartWare (Medtronic)	<0.20	CFD	[56]
Mechanical heart valves			
CarboMedics (Corcym)	0.05	Doppler	[21]
CarboMedics (Corcym) hinge	0.56	Laser Doppler velocimetry	[57]
Starr-Edwards (American Edwards Laboratories) silicone rubber ball	0.02	Doppler	[21]
Masters Series (St. Jude Medical)	0.16	PIV	[58]
On-X (Artivion)	0.16	PIV	[58]
Transcatheter valves			
Evolut (Medronic)	0.4-0.6	PIV	[59]
Sapien (Edwards Lifesciences)	0.3	PIV	[59]

CFD, computational fluid dynamics; PIV, particle imaging velocimetry; PTV, particle tracking velocimetry; Ref, reference; TKE, turbulent kinetic energy; VAD, ventricular assist device.

In a vascular anastomosis, flow can travel from a high-pressure artery to a low-pressure vein through a graft, whereas normal circulation must pass through arterioles, capillaries, and venules for the same pressure drop. As a result, blood velocity can be very high, with a *Re* of 900 to 1800. This can lead to transitional or weakly turbulent flow that can exist throughout the cardiac cycle, with reported coherent structures [63].

7 | ASSAYS TO STUDY TURBULENT FLOW WITH BLOOD SAMPLES

It can be challenging to study the effect of turbulence on blood in the laboratory due to the requirement for a high *Re* and the need for a pumping method that minimally impacts cells and proteins. For full-size vascular segments, the required volume of human blood becomes impractical for benchtop assays. This is one reason why *in vitro* flow loops for turbulence measurements are limited to a blood analog fluid or blood sourced from an animal. Alternatively, microfluidic channels have become commonplace to study blood, but flow is typically laminar due to characteristically small $Re \ll 1$ due to the small spatial scale of channels. A stenosis in these channels can lead to flow separation and increased *Re* at the throat, triggering flow instability but not likely turbulence [51,52,64]. Orbital shakers can be used as an alternative way to study turbulence in blood, but flow can be challenging to characterize in these systems. Viscometers have been useful for producing turbulence with relatively small quantities of blood. For example, a vane rheometer has been used to produce turbulence within a 7 mL sample, as demonstrated by a sudden increase in torque on the rheometer when increasing rotational speed [1]. The vane in this case involves 4 blades rotating with a 5.6 mm gap. For this specific setup, flow remains laminar at rotational rates less than 50 rad/s before becoming transitional and then turbulent at more than 200 rad/s, also predictable when estimating *Re* ($\rho\omega Rh/2\mu$), where ω is the angular velocity, *R* is the radius of the vane, and *h* is the gap. A cone-plate viscometer, traditionally used to create a uniform shear rate in a liquid, can lead to unstable flow if the cone angle and rotational velocity are sufficiently large, determined through flow visualization and a hot-film gauge [65]. In this study, the authors found that when the parameter $\rho R^2\omega\alpha^2/12\mu > 1$, the flow becomes unstable and potentially turbulent. This was confirmed by observing a sudden increase in torque on the cone. In this equation, *R* is the radius of the cone and a is the cone angle [66]. As illustrated in Figure 4B–D, a cup and bob rheometer can also lead to secondary flow and turbulence. There are limitations to rheometric approaches, including large surface area to volume ratios that can increase blood-material responses if not carefully blocked. There is also an air-liquid interface that could lead to protein accumulation. It should also be noted that turbulence is not uniform or isotropic (same in 3 dimensions) in these systems.

8 | INTERPLAY BETWEEN CELLS, PROTEINS, AND TURBULENCE

The implications of turbulence within the blood vessel are multifold. One challenge with identifying the impact of turbulence on blood is to

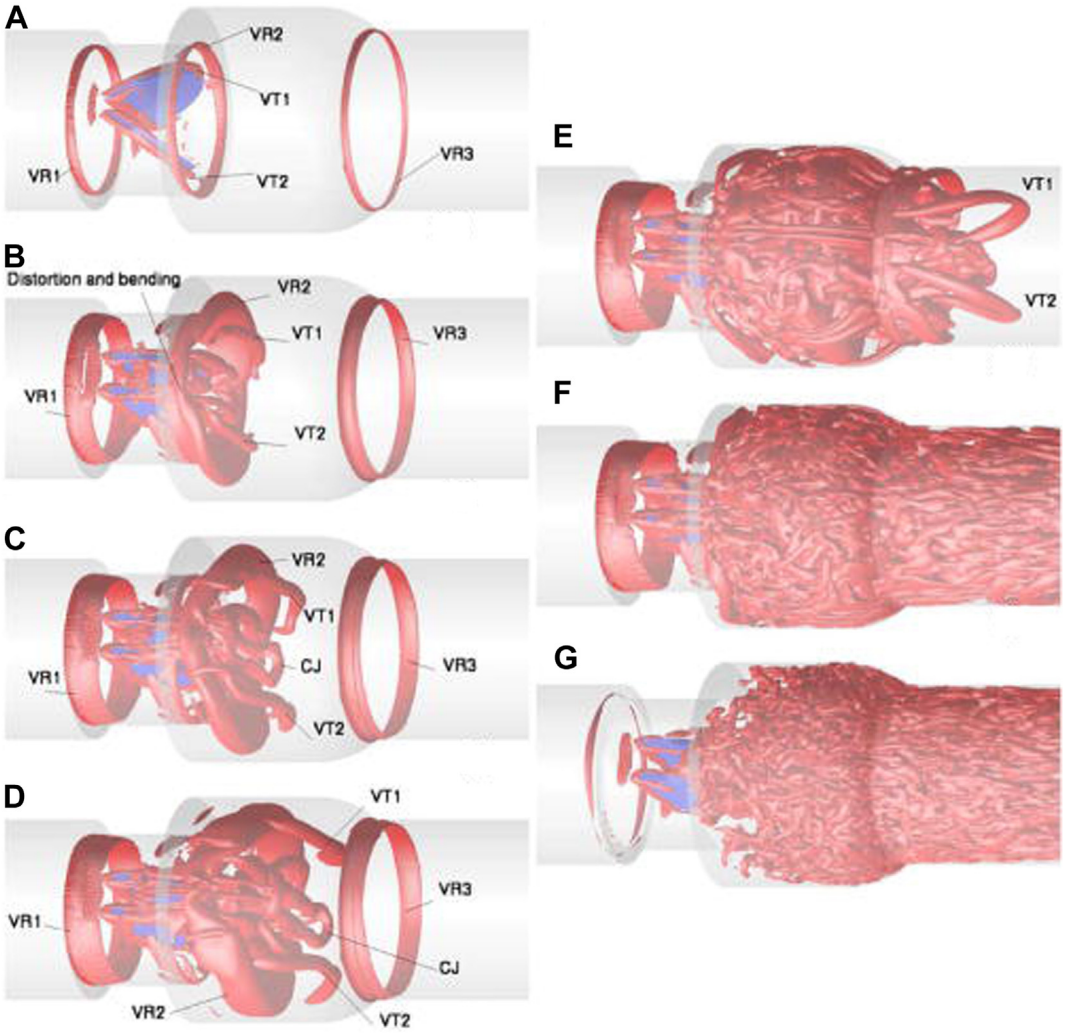

FIGURE 7 Three-dimensional coherent structures for a St. Jude Medical bileaflet mechanical heart valve based on a direct numerical simulation, validated with 2-dimensional particle imaging velocimetry experiments. The coherent structures are defined based on the q-criterion visualized (A) at the opening phase of the valve, (B–E) as fluid accelerates, (F) at peak systole, and (G) as flow decelerates. Reprinted from Dasi et al. [62] with permission. *CJ*, rectangular central orifice jet structure; *VR*, vortex ring 1, 2, or 3; *VT*, vortex tube, 1 or 2.

decouple effects from those of shear stress since high *Re* typically coincides with high shear stress. One approach is to increase the apparent viscosity of the blood sample for an otherwise turbulent flow, which lowers the *Re* but raises the shear stress. This approach has been used to demonstrate greater hemolysis in turbulent flow compared with laminar (Figure 8) [64]. Hemolysis, termed "blood damage" in some literature, can occur in turbulence with reported $RSS > \sim 350\text{-}450 Pa$ based on single-point measurements [67,68]. Hemolysis has deleterious effects since free hemoglobin is toxic to the endothelium and results in a cascade of responses, including nitric oxide scavenging, endothelial activation, oxidative stress, and barrier dysfunction [69]. In addition, the vascular endothelium is largely mechanoresponsive to turbulence [70]. Bovine aortic endothelial cells exhibit random orientation and become cuboidal when exposed to turbulence, with prolonged exposure causing cell loss and greater endothelial turnover [65]. Turbulence has also been proposed to increase the risk for thrombosis, which in part can relate to the damaged endothelium and hemolysis but may also result from other factors like shear-induced platelet activation and aggregation [3,9,10,71]. However, little literature exists on how platelets specifically respond to turbulence. Conversely, turbulence may also increase bleeding risk due to a loss of high-molecular-weight VWF multimers, with a Kolmogorov length scale that approaches 3 mm, a scale near the size of platelets, and large-molecular-weight multimers [1,14]. Although turbulence clearly affects cells and proteins in our blood, there is much to be discovered, motivating this Scientific and Standardization Committee (SSC) communication.

There is limited understanding of how RBCs can influence turbulence. RBCs, making up roughly half of the blood volume, play a major role in blood rheology. The effect of RBCs on turbulence becomes complicated at the scale of individual cells since RBCs rotate and deform in a dense suspension [72]. For turbulent blood flow, it is theoretically unlikely that eddies could reach a Kolmogorov length scale smaller than RBCs since the *Re* of plasma flowing between RBCs

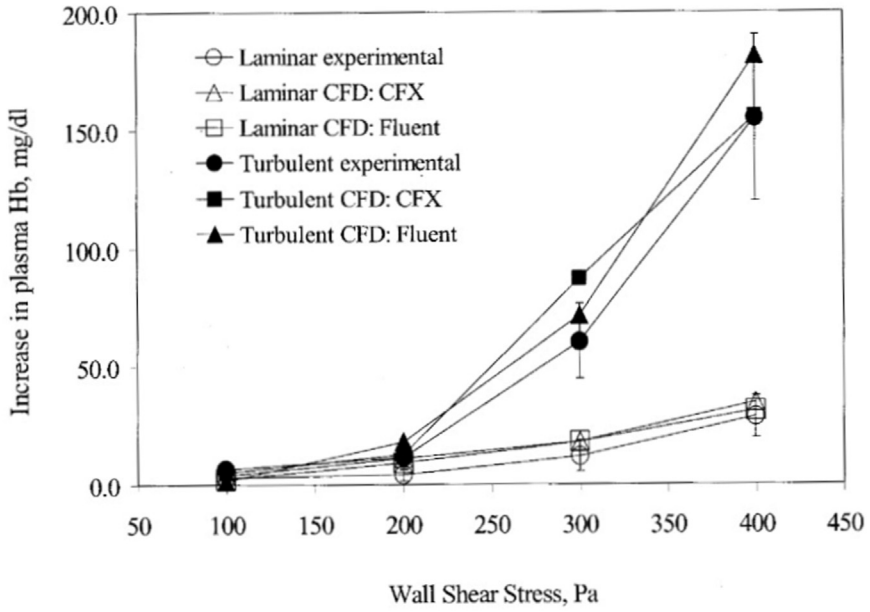

FIGURE 8 Hemolysis in a stenotic capillary tube demonstrated for laminar and turbulent flow for comparable wall shear stress conditions, reprinted from Kameneva et al. [64] with permission. The laminar sample contained Dextran-40 (Sigma Chemical Co., St. Louis, MO) to increase the viscosity to 6.3 ± 0.1 cP, whereas the turbulent sample had a viscosity of 2.0 ± 0.1 cP. Hematocrit in both cases was 24 ± 0.5%. *Hb*, hemoglobin; *CFD*, computational fluid dynamics; *CFX*, a commercial software for flow simulations.

is very small, bringing into question how turbulent flow affects platelets and plasma proteins [9,10]. Despite the potential lack of micron-scale eddies, RBCs can cause fluid behavior that is reminiscent of turbulence at the microscale, eg, high instantaneous shear stress, fluctuating velocities, and increased mixing, even under laminar conditions [9,73]. This could contribute to an early observation where the intensity of turbulence in the presence of RBCs was found to be over twice the amount from a viscosity-matched fluid without RBCs [74]. To gain insight into the cause, there is a need for microscale studies of blood rheology. *In vitro* experiments to study individual RBC behavior in a dense suspension is possible through transparent ghost RBCs (hemoglobin is removed) [72]. These experiments could be combined with PIV or PTV to quantify plasma flow between RBCs. It is noted, however, that microscale rheological behavior of ghosts may exhibit small differences from normal RBCs. *In silico* methods, alternatively, can capture flow behavior between simulated RBCs [75]. Despite these available methods, little is known about microscale rheology in blood, which may become even more complex with abnormal RBC morphologies, eg, sickled RBCs, spherocytes, and schistocytes.

9 | FINAL RECOMMENDATIONS AND FUTURE DIRECTIONS

This document is intended to provide some background on identifying and characterizing turbulence relative to laminar disturbed flow for

TABLE 4 Recommended measures and reporting of flow regimes.

Parameter	Expression in steady 1D	Meaning	Importance	Typical values and meaning in blood circulation
Re	$\frac{\rho \overline{U} D}{\mu}$	Inertial forces/viscous forces	Determines if flow is likely laminar, transitional, or turbulent	$Re \leq 2000$ laminar $2000 < Re \leq 4000$ transitional $Re > 4000$ turbulent
TI	$\frac{\sqrt{u^2}}{\sqrt{(\overline{U})^2}}$	Fluctuating velocity/mean velocity	Determines the relative amount of velocity fluctuation in flow	$TI \leq 1\%$ weak turbulence $1\% < TI \leq 5\%$ moderate turbulence $TI > 5\%$ high turbulence
TKE	$\frac{1}{2}\overline{u^2}$	Kinetic energy per unit mass from velocity fluctuations	Higher values mean increasing fluctuations in flow	$TKE < 0.1 \frac{m^2}{s^2}$ flow relatively stable $TKE > 0.1 \frac{m^2}{s^2}$ signs of highly unstable flow
RSS	$\rho \overline{uv}$	Remaining term when inserting Reynolds decomposition in governing equations of fluid mechanics	Used in engineering literature to quantify likelihood of "blood damage" typically defined by hemolysis	$RSS > 350$ more likely to cause hemolysis

D, diameter; μ, viscosity, 1D, 1 spatial dimension; ρ, density; Re, Reynolds number; RSS, Reynolds shear stress; TI, Turbulence intensity; TKE, turbulent kinetic energy; *U*, velocity; *u*, turbulent velocity fluctuation about the mean; $\overline{U}$, is the time-averaged velocity; $\overline{u}$, is the time-averaged turblent velocity fluctuation about the mean; $\overline{uv}$, is the time-averaged turbulent velocity fluctuation about the mean multiplied in two perpindicular directions.

TABLE 5 Summary of this Scientific and Standardization Committee communications.

Summarized key approaches, definitions, and considerations of turbulence	Description
Qualitative identification of turbulence	If a tracer or dye is used, it quickly mixes with surrounding fluid for turbulent flow. Flow patterns are not repeatable across periodic cycles or experiments.
Characteristics of transition to turbulence	High-frequency (>100 Hz) fluctuations in pressure and velocity. There is a sudden increase in the force required to drive a fluid as the velocity increases.
Disturbed flow or unstable laminar flow	Disturbed flow or unstable laminar flow is a type of laminar flow that exhibits secondary flow features, eg, a vortex, with repeatable tortuous fluid pathlines. This can occur with sudden changes in geometry, eg, aneurysms, stenosis, bifurcations, and sharp curvature.
Pitfalls when interpreting turbulent parameters in literature	The rigorous definition of turbulent parameters requires 3D measurements. Most techniques are 1D or 2D, so values when measuring turbulent parameters may be below actual values if all 3 dimensions could be measured. Measurement methods may have limited spatial or temporal resolution. Furthermore, measurements may vary in time and space, but maximum or average values are commonly reported, which can make it challenging to compare studies.
Assays to create turbulence with small sample volumes	High-speed cone and plate viscometers, vane rheometers, orbital shakers, and specialized devices utilizing external forces, eg, electric fields.
Effect of turbulence on hemostasis and thrombosis	Hemolysis, acquired von Willebrand syndrome, endothelial dysfunction, and potential increased platelet activation.

1D, 1-dimensional; 2D, 2-dimensional; 3D, 3-dimensional.

those working in the field of hemostasis and thrombosis. Flow should only be referenced as turbulent when the flow regime is rigorously defined with supporting evidence to remain consistent with other fields. A summary of recommended metrics to report when characterizing flow regimes is provided in Table 4. Further, to help identify and experiment with turbulence, a summary of information found in this SSC communication can be found in Table 5. Typically, blood flow is not turbulent, even though it may be disturbed and unstable. Blood flow may become turbulent in some pathologies, or when exposed to augmented flow found in mechanical circulatory support, or some mechanical heart valves. Therefore, there remains an important need to understand how turbulence can impact hemostasis and thrombosis. Although some studies have been performed, there are few that explicitly separate the effects of turbulence from fluid stress. In future work involving turbulent flow, it is recommended that fluid viscosity is augmented or that experiments are scaled in size to help distinguish effects of turbulence from fluid stress. Furthermore, the role of turbulence on platelet activation, adhesion, and aggregation remains poorly defined but could provide insight into the bleeding and thrombotic complications seen in some pathologies. Similarly, turbulence could affect many other cells and proteins but generally remains understudied in blood. Further complicating the role of turbulence is the dense suspension of cells and proteins that exist in blood. There remains little known on how turbulent flow affects the microscale environment compared with homogenous, uniform liquids or how cells and proteins deform to influence small eddies in turbulent flow. These topics provide rich future directions. Overall, turbulence remains an important topic in hemostasis and thrombosis, but future studies are needed to help elucidate specific relationships between turbulence and blood responses.

ACKNOWLEDGMENTS

Figure 3 was created with BioRender.com.

AUTHOR CONTRIBUTIONS

D.L.B. and E.E.G. initiated the SSC project and the manuscript. All authors significantly contributed to the writing.

DECLARATION OF COMPETING INTERESTS

There are no competing interests to disclose.

X

David L. Bark X @Bark_Lab

REFERENCES

[1] Bortot M, Ashworth K, Sharifi A, Walker F, Crawford NC, Neeves KB, Bark Jr D, Di Paola J. Turbulent flow promotes cleavage of VWF (von Willebrand factor) by ADAMTS13 (a disintegrin and metalloproteinase with a thrombospondin type-1 motif, member 13). *Arterioscler Thromb Vasc Biol*. 2019;39:1831–42.

[2] Stein PD, Sabbah HN. Turbulent blood flow in the ascending aorta of humans with normal and diseased aortic valves. *Circ Res*. 1976;39:58–65.

[3] Becker RC, Eisenberg P, Turpie AG. Pathobiologic features and prevention of thrombotic complications associated with prosthetic heart valves: fundamental principles and the contribution of platelets and thrombin. *Am Heart J*. 2001;141:1025–37.

[4] Nesbitt WS, Westein E, Tovar-Lopez FJ, Tolouei E, Mitchell A, Fu J, Carberry J, Fouras A, Jackson SP. A shear gradient–dependent platelet aggregation mechanism drives thrombus formation. *Nat Med*. 2009;15:665–73.

[5] Moody LF. Friction factors for pipe flow. *Trans ASME*. 1944;66:671–8.

[6] Aider AA, Skali S, Brancher JP. Laminar-turbulent transition in Taylor-Dean flow. *J Phys Conf Ser*. 2005;14:118. https://doi.org/10.1088/1742-6596/14/1/015

[7] Bharadvaj BK, Mabon RF, Giddens DP. Steady flow in a model of the human carotid bifurcation. Part I—flow visualization. *J Biomech*. 1982;15:349–62.

[8] Taylor GI. Experiments with rotating fluids. *Proc R Soc Lond A Math Phys Sci*. 1921;100:114–21.

[9] Morshed KN, Bark Jr D, Forleo M, Dasi LP. Theory to predict shear stress on cells in turbulent blood flow. *PLoS One*. 2014;9:e105357. https://doi.org/10.1371/journal.pone.0105357

[10] Antiga L, Steinman DA. Rethinking turbulence in blood. *Biorheology*. 2009;46:77–81.

[11] Pope SB. *Turbulent flows*. Cambridge: Cambridge University Press; 2000.

[12] Dimotakis PE. Turbulent mixing. *Annu Rev Fluid Mech*. 2005;37:329–56.

[13] Zhou Y, Schroeder CM. Single polymer dynamics under large amplitude oscillatory extension. *Phys Rev Fluids*. 2016;1:053301. https://doi.org/10.1103/PhysRevFluids.1.053301

[14] Sharifi A, Bark D. Mechanical forces impacting cleavage of von Willebrand factor in laminar and turbulent blood flow. *Fluids*. 2021;6:67. https://doi.org/10.3390/fluids6020067

[15] Kuethe DO. Measuring distributions of diffusivity in turbulent fluids with magnetic-resonance imaging. *Phys Rev A Gen Phys*. 1989;40:4542–51.

[16] Kuethe DO, Gao JH. NMR signal loss from turbulence: models of time dependence compared with data. *Phys Rev E Stat Phys Plasmas Fluids Relat Interdiscip Topics*. 1995;51:3252–62.

[17] Dyverfeldt P, Sigfridsson A, Kvitting JPE, Ebbers T. Quantification of intravoxel velocity standard deviation and turbulence intensity by generalizing phase-contrast MRI. *Magn Reson Med*. 2006;56:850–8.

[18] De Gennes PG. Theory of spin echoes in a turbulent fluid. *Phys Lett A*. 1969;29:20–1.

[19] Elkins CJ, Alley MT, Saetran L, Eaton JK. Three-dimensional magnetic resonance velocimetry measurements of turbulence quantities in complex flow. *Exp Fluids*. 2009;46:285–96.

[20] Dyverfeldt P, Gårdhagen R, Sigfridsson A, Karlsson M, Ebbers T. On MRI turbulence quantification. *Magn Reson Imaging*. 2009;27:913–22.

[21] Nygaard H, Paulsen PK, Hasenkam JM, Pedersen EM, Rovsing PE. Turbulent stresses downstream of three mechanical aortic valve prostheses in human beings. *J Thorac Cardiovasc Surg*. 1994;107:438–46.

[22] Isaaz K, Bruntz JF, Da Costa A, Winninger D, Cerisier A, de Chillou C, Sadoul N, Lamaud M, Ethevenot G, Aliot E. Noninvasive quantitation of blood flow turbulence in patients with aortic valve disease using online digital computer analysis of Doppler velocity data. *J Am Soc Echocardiogr*. 2003;16:965–74.

[23] Liu JS, Lu PC, Chu SH. Turbulence characteristics downstream of bileaflet aortic valve prostheses. *J Biomech Eng*. 2000;122:118–24.

[24] Le TB, Sotiropoulos F. On the three-dimensional vortical structure of early diastolic flow in a patient-specific left ventricle. *Eur J Mech B Fluids*. 2012;35:20–4.

[25] Chnafa C, Mendez S, Nicoud F. Image-based large-eddy simulation in a realistic left heart. *Comput Fluids*. 2014;94:173–87.

[26] Domenichini F, Pedrizzetti G, Baccani B. Three-dimensional filling flow into a model left ventricle. *J Fluid Mech*. 2005;539:179–98.

[27] Chnafa C, Mendez S, Nicoud F. Image-based simulations show important flow fluctuations in a normal left ventricle: what could be the implications? *Ann Biomed Eng*. 2016;44:3346–58.

[28] Gülan U, Rossi VA, Gotschy A, Saguner AM, Manka R, Brunckhorst CB, Duru F, Schmied CM, Niederseer D. A comparative study on the analysis of hemodynamics in the athlete's heart. *Sci Rep*. 2022;12:16666. https://doi.org/10.1038/s41598-022-20839-8

[29] Gülan U, Saguner AM, Akdis D, Gotschy A, Tanner FC, Kozerke S, Manka R, Brunckhorst C, Holzner M, Duru F. Hemodynamic changes in the right ventricle induced by variations of cardiac output: a possible mechanism for arrhythmia occurrence in the outflow tract. *Sci Rep*. 2019;9:100. https://doi.org/10.1038/s41598-018-36614-7

[30] Saikrishnan N, Yap CH, Milligan NC, Vasilyev NV, Yoganathan AP. *In vitro* characterization of bicuspid aortic valve hemodynamics using particle image velocimetry. *Ann Biomed Eng*. 2012;40:1760–75.

[31] Ha H, Ziegler M, Welander M, Bjarnegård N, Carlhäll CJ, Lindenberger M, Länne T, Ebbers T, Dyverfeldt P. Age-related vascular changes affect turbulence in aortic blood flow. *Front Physiol*. 2018;9:36. https://doi.org/10.3389/fphys.2018.00036

[32] Yamaguchi T, Kikkawa S, Yoshikawa T, Tanishita K, Sugawara M. Measurement of turbulence intensity in the center of the canine ascending aorta with a hot-film anemometer. *J Biomech Eng*. 1983;105:177–87.

[33] Valen-Sendstad K, Piccinelli M, Steinman DA. High-resolution computational fluid dynamics detects flow instabilities in the carotid siphon: implications for aneurysm initiation and rupture? *J Biomech*. 2014;47:3210–6.

[34] Buchmann NA, Atkinson C, Jeremy MC, Soria J. Tomographic particle image velocimetry investigation of the flow in a modeled human carotid artery bifurcation. *Exp Fluids*. 2011;50:1131–51.

[35] Dyverfeldt P, Kvitting JPE, Carlhäll CJ, Boano G, Sigfridsson A, Hermansson U, Bolger AF, Engvall J, Ebbers T. Hemodynamic aspects of mitral regurgitation assessed by generalized phase-contrast MRI. *J Magn Reson Imaging*. 2011;33:582–8.

[36] Dyverfeldt P, Hope MD, Tseng EE, Saloner D. Magnetic resonance measurement of turbulent kinetic energy for the estimation of irreversible pressure loss in aortic stenosis. *JACC Cardiovasc Imaging*. 2013;6:64–71.

[37] Binter C, Gotschy A, Sündermann SH, Frank M, Tanner FC, Lüscher TF, Manka R, Kozerke S. Turbulent kinetic energy assessed by multipoint 4-dimensional flow magnetic resonance imaging provides additional information relative to echocardiography for the determination of aortic stenosis severity. *Circ Cardiovasc Imaging*. 2017;10:e005486. https://doi.org/10.1161/CIRCIMAGING.116.005486

[38] Ha H, Kim GB, Kweon J, Huh HK, Lee SJ, Koo HJ, Kang JW, Lim TH, Kim DH, Kim YH, Kim N, Yang DH. Turbulent kinetic energy measurement using phase contrast MRI for estimating the post-stenotic pressure drop: *in vitro* validation and clinical application. *PLoS One*. 2016;11:e0151540. https://doi.org/10.1371/journal.pone.0151540

[39] Dyverfeldt P, Kvitting JPE, Sigfridsson A, Engvall J, Bolger AF, Ebbers T. Assessment of fluctuating velocities in disturbed cardiovascular blood flow: *in vivo* feasibility of generalized phase-contrast MRI. *J Magn Reson Imaging*. 2008;28:655–63.

[40] Lantz J, Ebbers T, Engvall J, Karlsson M. Numerical and experimental assessment of turbulent kinetic energy in an aortic coarctation. *J Biomech*. 2013;46:1851–8.

[41] Andersson M, Karlsson M. Characterization of anisotropic turbulence behavior in pulsatile blood flow. *Biomech Model Mechanobiol*. 2021;20:491–506.

[42] Arzani A, Dyverfeldt P, Ebbers T, Shadden SC. *In vivo* validation of numerical prediction for turbulence intensity in an aortic coarctation. *Ann Biomed Eng*. 2012;40:860–70.

[43] Lee SE, Lee SW, Fischer PF, Bassiouny HS, Loth F. Direct numerical simulation of transitional flow in a stenosed carotid bifurcation. *J Biomech*. 2008;41:2551–61.

[44] Ziegler M, Alfraeus J, Good E, Engvall J, De Muinck E, Dyverfeldt P. Exploring the relationships between hemodynamic stresses in the carotid arteries. *Front Cardiovasc Med*. 2021;7:617755. https://doi.org/10.3389/fcvm.2020.617755

[45] Freidoonimehr N, Arjomandi M, Sedaghatizadeh N, Chin R, Zander A. Transitional turbulent flow in a stenosed coronary artery

with a physiological pulsatile flow. *Int J Numer Method Biomed Eng*. 2020;36:e3347. https://doi.org/10.1002/cnm.3347

[46] Peterson SD, Plesniak MW. The influence of inlet velocity profile and secondary flow on pulsatile flow in a model artery with stenosis. *J Fluid Mech*. 2008;616:263–301.

[47] Zajac J, Eriksson J, Dyverfeldt P, Bolger AF, Ebbers T, Carlhäll CJ. Turbulent kinetic energy in normal and myopathic left ventricles. *J Magn Reson Imaging*. 2015;41:1021–9.

[48] Kronborg J, Svelander F, Eriksson-Lidbrink S, Lindström L, Homs-Pons C, Lucor D, Hoffman J. Computational analysis of flow structures in turbulent ventricular blood flow associated with mitral valve intervention. *Front Physiol*. 2022;13:806534. https://doi.org/10.3389/fphys.2022.806534

[49] Sabbah HN, Walburn FJ, Stein PD. Patterns of flow in the left coronary artery. *J Biomech Eng*. 1984;106:272–9.

[50] Mahalingam A, Gawandalkar UU, Kini G, Buradi A, Araki T, Ikeda N, Nicolaides A, Laird JR, Saba L, Suri JS. Numerical analysis of the effect of turbulence transition on the hemodynamic parameters in human coronary arteries. *Cardiovasc Diagn Ther*. 2016;6:208–20.

[51] Young DF, Tsai FY. Flow characteristics in models of arterial stenoses. II. Unsteady flow. *J Biomech*. 1973;6:547–59.

[52] Young DF, Tsai FY. Flow characteristics in models of arterial stenoses. I. Steady flow. *J Biomech*. 1973;6:395–410.

[53] Bark Jr DL, Ku DN. Wall shear over high degree stenoses pertinent to atherothrombosis. *J Biomech*. 2010;43:2970–7.

[54] Wiegmann L, Thamsen B, De Zélicourt D, Granegger M, Boës S, Schmid Daners M, Meboldt M, Kurtcuoglu V. Fluid dynamics in the HeartMate 3: influence of the artificial pulse feature and residual cardiac pulsation. *Artif Organs*. 2019;43:363–76.

[55] Thamsen B, Gülan U, Wiegmann L, Loosli C, Schmid Daners M, Kurtcuoglu V, Holzner M, Meboldt M. Assessment of the flow field in the HeartMate 3 using three-dimensional particle tracking velocimetry and comparison to computational fluid dynamics. *ASAIO J*. 2020;66:173–82.

[56] Thamsen B, Blümel B, Schaller J, Paschereit CO, Affeld K, Goubergrits L, Kertzscher U. Numerical analysis of blood damage potential of the HeartMate II and HeartWare HVAD rotary blood pumps. *Artif Organs*. 2015;39:651–9.

[57] Leo HL, He Z, Ellis JT, Yoganathan AP. Microflow fields in the hinge region of the CarboMedics bileaflet mechanical heart valve design. *J Thorac Cardiovasc Surg*. 2002;124:561–74.

[58] Hatoum H, Maureira P, Dasi LP. A turbulence *in vitro* assessment of On-X and St Jude Medical prostheses. *J Thorac Cardiovasc Surg*. 2020;159:88–97.

[59] Hatoum H, Yousefi A, Lilly S, Maureira P, Crestanello J, Dasi LP. An *in vitro* evaluation of turbulence after transcatheter aortic valve implantation. *J Thorac Cardiovasc Surg*. 2018;156:1837–48.

[60] Yoganathan AP, Chandran K, Sotiropoulos F. Flow in prosthetic heart valves: state-of-the-art and future directions. *Ann Biomed Eng*. 2005;33:1689–94.

[61] Li CP, Chen SF, Lo CW, Lu PC. Turbulence characteristics downstream of a new trileaflet mechanical heart valve. *ASAIO J*. 2011;57:188–96.

[62] Dasi LP, Ge L, Simon HA, Sotiropoulos F, Yoganathan AP. Vorticity dynamics of a bileaflet mechanical heart valve in an axisymmetric aorta. *Phys Fluids*. 2007;19:067105. https://doi.org/10.1063/1.2743261

[63] Lee SW, Fischer PF, Loth F, Royston T, Grogan JK, Bassiouny HS. Flow-induced vein-wall vibration in an arteriovenous graft. *J Fluids Struct*. 2005;20:837–52.

[64] Kameneva MV, Burgreen GW, Kono K, Repko B, Antaki JF, Umezu M. Effects of turbulent stresses upon mechanical hemolysis: experimental and computational analysis. *ASAIO J*. 2004;50:418–23.

[65] Davies PF, Remuzzi A, Gordon EJ, Dewey Jr CF, Gimbrone Jr MA. Turbulent fluid shear stress induces vascular endothelial cell turnover *in vitro*. *Proc Natl Acad Sci U S A*. 1986;83:2114–7.

[66] Dewey Jr CF, Bussolari SR, Gimbrone Jr MA, Davies PF. The dynamic response of vascular endothelial cells to fluid shear stress. *J Biomech Eng*. 1981;103:177–85.

[67] Sallam AM, Hwang NH. Human red blood cell hemolysis in a turbulent shear flow: contribution of Reynolds shear stresses. *Biorheology*. 1984;21:783–97.

[68] Yoganathan AP, Woo YR, Sung HW. Turbulent shear stress measurements in the vicinity of aortic heart valve prostheses. *J Biomech*. 1986;19:433–42.

[69] Meegan JE, Bastarache JA, Ware LB. Toxic effects of cell-free hemoglobin on the microvascular endothelium: implications for pulmonary and nonpulmonary organ dysfunction. *Am J Physiol Lung Cell Mol Physiol*. 2021;321:L429–39.

[70] Humphrey JD, Schwartz MA, Tellides G, Milewicz DM. Role of mechanotransduction in vascular biology: focus on thoracic aortic aneurysms and dissections. *Circ Res*. 2015;116:1448–61.

[71] Stein PD, Sabbah HN. Measured turbulence and its effect on thrombus formation. *Circ Res*. 1974;35:608–14.

[72] Goldsmith HL, Marlow JC. Flow behavior of erythrocytes. II. Particle motions in concentrated suspensions of ghost cells. *J Colloid Interface Sci*. 1979;71:383–407.

[73] Wang NHL, Keller KH. Augmented transport of extracellular solutes in concentrated erythrocyte suspensions in Couette flow. *J Colloid Interface Sci*. 1985;103:210–25.

[74] Stein PD, Sabbah HN, Blick EF. Contribution of erythrocytes to turbulent blood flow. *Biorheology*. 1975;12:293–9.

[75] Liu Z, Clausen JR, Rao RR, Aidun CK. Nanoparticle diffusion in sheared cellular blood flow. *J Fluid Mech*. 2019;871:636–67.